FunMaps: a toolbox for parcellating functional brain networks using resting-state functional MRI data

Authors and addresses:
Jiayu Shao, BS[1], Stephen J. Gotts, PhD[1], Alex Martin, PhD[1], Andrew S. Persichetti, PhD[1*]
[1]Section on Cognitive Neuropsychology, Laboratory of Brain and Cognition, National Institute of Mental Health, National Institutes of Health, Bethesda, Maryland 20892

Corresponding author:
Andrew S. Persichetti
Laboratory of Brain and Cognition, NIMH/NIH
10 Center Drive, MSC 1366
Building 10, Room 4C104
Bethesda, MD 20892,
Office: 301-451-2223
persichettias@nih.gov

Author contributions
A.S.P., S.J.G., J.S. and A.M. designed research; A.S.P, J.S., and S.J.G. performed research and analyzed data; J.S., A.S.P., S.J.G. and A.M. wrote the paper.

Keywords: resting-state, fMRI, functional connectivity, parcellation

ABSTRACT

Parcellations of resting-state functional magnetic resonance imaging (rs-fMRI) data are widely used to create topographical maps of functional networks in the human brain. While such network maps are highly useful for studying brain organization and function, they usually require large sample sizes to make them, thus creating practical limitations for researchers that would like to carry out parcellations on data collected in their labs. Furthermore, it can be difficult to quantitatively evaluate the results of a parcellation since networks are usually identified using a clustering algorithm, like principal components analysis, on the results of a single group-averaged connectivity map. To address these challenges, we developed the FunMaps toolbox: a parcellation routine that intrinsically incorporates stability and replicability of the parcellation by keeping only network distinctions that agree across halves of the data over multiple random iterations. Here, we demonstrate the efficacy and flexibility of FunMaps, while describing step-by-step instructions for running the program. The FunMaps toolbox is publicly available on GitHub (https://github.com/persichetti-lab/FunMaps). It includes source code for running the parcellation and auxiliary code for preparing data, evaluating the parcellation, and displaying the results.

INTRODUCTION

Functional parcellations of resting state fMRI (rs-fMRI) data provide useful maps of functional networks in human cortex (Glasser et al., 2016; Power et al., 2011; Yeo et al., 2011). By subdividing the cortex into a topography of functional units, neuroscientists can more easily identify brain areas and networks that are relevant to a particular research question, while also forming new hypotheses based on the network architecture. Furthermore, individual parcels from a functional network map provide a valid means of reducing the number of units in a statistical test (from voxels to parcels) and identifying regions of interest for seed-based connectivity and task-based experiments. Parcellation algorithms can also be used to create group-specific topographies that can be used to compare network characteristics between clinical populations and matched controls (Persichetti et al., 2023). However, creating group-specific functional parcellations is often not feasible with commonly used parcellation methods because they require sample sizes that are much larger than the typical dataset collected in a lab to ensure that the resultant network maps are stable and reliable.

In this paper, we introduce a software toolbox, called FunMaps, that we developed to perform flexible and data-driven functional parcellations of the brain to derive network maps with relatively small datasets collected in individual labs. FunMaps incorporates stability measures by searching for networks across random split halves of the data over multiple iterations and then keeping only networks that are present in both halves across several iterations (Persichetti et al., 2021, 2023). The FunMaps parcellation tool comprises several steps that are controlled through a wrapper function.

We will walk through the steps of the parcellation, how to enter the desired parameters into the wrapper, and how to evaluate the output at each step. We will show step-by-step results to highlight some of the ways that FunMaps can be applied to rs-fMRI data. In addition, we will describe and evaluate several auxiliary functions included in the FunMaps toolbox. FunMaps can be downloaded for free on Github (https://github.com/persichetti-lab/FunMaps). The Github page also includes a link to a sample dataset (https://osf.io/we8k3) for users who want to try running the toolbox on data used in this paper.

RESULTS

Brief overview. The FunMaps toolbox is a Matlab based pipeline that also uses AFNI fMRI analysis software (Cox, 1996), and the graph theory-based Infomap algorithm for community detection (Rosvall & Bergstrom, 2008, 2011). Instructions for downloading the toolbox dependencies can be found on the FunMaps GitHub page. All functions in the main pipeline are controlled through a wrapper function (funmapsWrapper.m) that allows the researcher to update the necessary variables for each step in the pipeline and execute them from one script. Below we will describe each step of the pipeline and which variables coincide with them when applicable (see Table 1 for a schematic of the directory structure and output of FunMaps).

Step 0: Data and materials needed to run FunMaps. Before running FunMaps, you will need to make an experiment directory with two subdirectories: One called “brains” that contains the cleaned rs-fMRI timeseries data for all participants in the study and

another directory called “masks” that contains two types of masks in the native resolution of the timeseries data (Figure 1A). The toolbox expects all initial brain data and masks to be in NIfTI format and to be in a standard volumetric space (e.g., our data are in Talairach space – (Talairach et al., 1997). The first type of mask is the region of interest (ROI) mask, which consists of all the voxels within the brain region(s) that you want to parcellate. The ROI mask can range in size from a small region of study (e.g., the anterior portion of the temporal lobes – Persichetti et al., 2021) to the whole brain (Persichetti et al., 2023). If your ROI includes both cortical and subcortical voxels, then we recommend separating the ROI mask into cortical and subcortical masks. The pipeline can handle multiple ROI masks at a time, if necessary. The cortical and subcortical ROI’s will be parcellated separately and then combined at a later step in the pipeline. The second type of mask is the target mask, which will often be a whole-brain mask, but you can also decide to exclude voxels that are in your ROI mask – e.g., if you have a small ROI mask and you do not want to use voxel-to-voxel correlations from within the ROI (see Persichetti et al., 2021 for an example of this approach). Additionally, we recommend removing voxels with poor temporal signal-to-noise ratio (tSNR) and prominent blood vessel signal from both types of masks. The toolbox includes an auxiliary function (cleanMask.m) that removes from each mask voxels with poor tSNR and prominent blood vessel signals (identified from a standard deviation map of the volume registered EPI data – (Kalcher et al., 2015).

Step 1: Extract voxelwise timeseries data from each mask (dumpTS.m). The *dumpTS* function downsamples the data and masks to a lower spatial resolution, then

extracts voxelwise time series data from the rs-fMRI volumes and saves it into text files. Downsampling the data before starting the parcellation saves lots of time without sacrificing performance of the parcellation routine. For example, in Persichetti et al. (2023), we started with 2 mm^3 resolution voxels, then downsampled the whole-brain target mask and the cortical ROI mask to 6 mm^3 resolution, while the subcortical ROI mask was downsampled to 3 mm^3 resolution because of its smaller starting volume. Users can choose to omit or modify the degree of down sampling to match the needs of their data, using the variables *roiDownDimArray* and *targetDownDim* in the wrapper. Next, to lower data storage requirements, the ROI and target masks are used to extract voxelwise time series data from the rs-fMRI volumes and save it into 1D vectors. Thus, the output of this step will be new downsampled masks in the *masks* directory (if downsampling is indicated in the wrapper, highly recommended) and a new subdirectory, named *timeseries*, that contains 1D text files of voxelwise rs-fMRI timeseries data from each participant and each mask in the desired spatial resolution.

Step 2: Create random split-half datasets (genSplits.m). The *genSplits* function randomly splits the participant data into two equal groups, calculates the voxelwise correlation matrices between each ROI mask and the target mask data (done separately for each ROI mask) for each participant, then combines the correlation matrices from all participants in each split-half group to create a group-averaged correlation matrix in each half of the data. This process is repeated over several iterations (we recommend ten split-half iterations as a good tradeoff between finding stability and minimizing computation time), each time randomly splitting the group of

participants into two equal sized groups. The group-averaged ROI x target matrix from each half and each iteration is then made square by calculating the column-wise correlation, yielding an ROI-voxels x ROI-voxels matrix that reflects the similarity of connectivity patterns from ROI voxels to the voxels in the target mask. The final step formats the matrices to be compatible with the InfoMap algorithm that will be used in the next step of the pipeline. Specifically, the real-valued correlation matrices are thresholded into binary (0 or 1) undirected matrices at a range of threshold values representing the top percentages of connections and then converted to the Pajek file format. In the examples used in this paper, we used the following thresholds: 50, 60, 70, 80, 85, 90, 91, 92, 93, 94, 95, 96, 97, 98, 99, and 99.5% (indicated in the wrapper by the variable *testThreshArray* as proportions – e.g., 0.5, 0.6, 0.7, etc.). We used this wide range of thresholds to give the reader a sense of the effect thresholding has on the parcellation routine. However, we recommend that users constrain this range to something closer to steps of 3% between 80-95% to save time, since we have consistently found that ideal thresholds to be 85% for subcortical masks and 90% for cortical masks.

Step 3: Create network prototypes (genClusters.m). The *genClusters* function searches for network prototypes in the thresholded matrices of each split-half group using the InfoMap algorithm to form optimal two-level partitions (FunMaps searches for the optimal solution over 100 searches on each split-half iteration). Prototypes found in each half of the data are required to replicate across halves in each iteration. Specifically, in each iteration, a prototype is counted as replicating if the Dice coefficient

[$(2|X \cap Y| \,/\, (|X| + |Y|)$] is greater than 0.5 and the volume of the intersecting voxels for the prototype is at least 2% of the ROI mask size. Network prototypes that meet these criteria are retained in each iteration. After repeating the above steps for all iterations, an agreement matrix is created, such that each cell reflects the proportion of iterations in which two voxels were part of the same network prototype that agreed across the split halves. Thus, if two voxels were part of a prototype that was present in eight out of ten iterations, then that cell of the matrix would get a value of 0.8 to indicate that it was present in 80% of the iterations. The matrix is then thresholded such that two voxels are required to be part of the same prototype in at least 50% of the iterations. It is important to note that at this step the matrix has lost the prototype labels and is simply a binarized matrix reflecting generic network prototype membership across voxels. The voxels will be relabeled in the next step of the toolbox (*genParcels*).

The above process is completed for all thresholds indicated in the prior step and agreement curves for each ROI are constructed across thresholds (Figure 1B). The agreement curves can be evaluated to find the threshold with the desired split-half agreement in brain coverage (i.e., the percentage of voxels assigned to a prototype at each threshold) and the total number of prototypes retained. At this point, the program pauses and asks the user to enter on the command line which threshold should be used for each ROI mask. Once the user enters the desired threshold for each ROI mask on the command line, the program resumes the parcellation for those thresholds only. In the example presented here, we chose 90% for the cortical mask and 85% as the threshold for the subcortical mask because we have consistently found these to be ideal thresholds for these types of masks (Figure 1B). However, it is critical that users

evaluate the agreement curves and decide for themselves how they want to proceed, since the optimal threshold will be dependent on features of each dataset, such as sample size and tSNR. In addition to evaluating the agreement curves, the user should run the auxiliary function called *undumpPrototypes.m* that is provided in the FunMaps toolbox to map the prototypes (in the downsampled space) at a given threshold onto the brain volume (Figure 1C). It is important to note that the number of prototypes that are mapped to the volume may differ slightly from the number indicated on the agreement curve because each prototype must cover at least 2% of the ROI mask. The volumetric prototypes are saved in a text file named with the ROI mask and the threshold value (e.g., cort*ex_prototypeNets_90.1D*) and as a NIfTI formatted brain volume with the same name. The resultant brain map will give the user a good idea about whether the parcellation solution at the selected threshold is reasonable or not.

Step 4: Assign network labels in the original volume space (genParcels.m). The *genParcels* function assigns final network labels to each voxel in the original spatial resolution. To save time, this step is completed entirely on vectors in the 1D text file format. The network labels will be mapped onto a brain volume in the next step. First, the program iterates through the timeseries data for each ROI mask in each participant and makes a correlation matrix that reflects the pattern of functional connectivity between each voxel in the ROI mask with all voxels in the target mask. These correlation matrices are then averaged across participants in the downsampled space. These voxelwise patterns of connectivity are then assigned prototype labels, and voxels from the same prototype are averaged together to get an average pattern of brain

connectivity for each prototype. The average pattern of brain connectivity for each prototype from all ROI masks is then correlated with the pattern from every voxel across the brain in the original spatial resolution of the data. Thus, a prototype that originated in the subcortical ROI mask can include network voxels in the cortex, and vice versa. In a winner-takes-all approach, each voxel is given the label of the network prototype that explains the most variance in that voxel. However, as a final quality assurance step, the winning network prototype must explain at least 50% of the variance (i.e., $R^2 > 0.5$) in the functional connectivity pattern of a given voxel for it to get a final network label, otherwise the voxel does not get a label at this step. We do this to avoid giving "noise voxels" (e.g., voxels with prominent blood vessel signal) a network label. At the end of this step, the final network labels are saved in a 1D text file along with the coordinates of all brain voxels in the original spatial resolution of the data. In the next and final step of the program, each voxel will be given a network label while remapping the data into the brain volume.

Step 5: Create a final volume that includes all networks (genVolume.m). The *genVolume* function maps the network labels assigned to each voxel in the original spatial resolution of the data onto the brain volume in the NIfTI (.nii) file format. At this step, every voxel that was not assigned a network label in the previous step is given a label using nearest-neighbor interpolation. The map of brain-wide functional networks provided by FunMaps is now complete and the final volumetric rendering of the whole-brain network parcellation can be easily visualized (Figure 2A). The toolbox also includes an auxiliary function called *vol2surf.m* that uses the HCP Connectome

Workbench (Marcus et al., 2013) to create a surface rendering of the cortical networks (Figure 2B). Instructions for downloading the Workbench software are on the FunMaps GitHub page.

Focused parcellations. In addition to parcellating the whole brain, FunMaps can be used to parcellate select brain regions. In this way, the toolbox can be used to find finer grained parcellations within each network found in the first use of FunMaps. It can also be used to parcellate an a priori brain region – e.g., in a recently published paper, we used the FunMaps toolbox to parcellate the anterior portions of the temporal lobes (i.e. the ATL – Persichetti et al, 2021). An example of both uses of FunMaps can be found in the above-mentioned paper, in which we used it to find functional network boundaries in the ATL. Specifically, in that paper, we focused our parcellation on a mask that covered the bilateral ATL and another that included the hippocampus and amygdala (Figure 3). The initial parcellation yielded eight parcels across the cortical and subcortical masks (Figure 3A). We then parcellated each cortical parcel again and ended with a total of 34 distinct functional networks in the ATL (Figure 3B). We provided further analyses to demonstrate that the parcellation identified functionally specific brain networks (see Persichetti et al., 2021 for details). Additionally, results from this paper demonstrated that focusing our parcellation routine specifically on the hippocampus and amygdala identified expected functional boundaries in these structures – separating the amygdala from the hippocampus and further dividing the hippocampus into tail, body, and head (Figure 3C). The divisions within the hippocampus are consistent with an anterior-to-posterior functional gradient within the hippocampus (Fanselow & Dong, 2010; Grady,

2020; Nadel et al., 2013; Poppenk et al., 2013; Ranganath & Ritchey, 2012; Sekeres et al., 2018). Thus, the FunMaps toolbox allows users to control the granularity of the network maps by refocusing the parcellation routine on more restricted brain volumes.

Sample size. Another major benefit of the FunMaps toolbox is that it requires a very small sample size compared to most parcellation methods. This is excellent news for researchers that want to create maps of functional brain networks that are specific to a dataset that was collected in their lab. This is especially useful for researchers interested in creating functional network maps that are specific to a clinical population. For example, we recently used the FunMaps toolbox and data collected in our lab to create whole-brain functional network maps in a group of seventy individuals with autism spectrum disorder (ASD) and a group of seventy data-quality-matched typically developing (TD) control participants (Persichetti et al., 2023). Each participant in this study completed just one rest run of eight minutes and ten seconds in the scanner. We were able to identify the most stable parcellation solution in both groups using agreement curves that reflected the proportion of brain coverage and the number of found networks across a series of matrix thresholds. Our ability to find a stable parcellation of the ASD group allowed us to run a series of analyses that suggest patterns of network connectivity between the neocortex and the cerebellum, subcortical structures, and hippocampus are atypical in ASD individuals. Critically, the novel parcellation routine implemented by the FunMaps toolbox allowed us to create a functional network map that was specific to a clinical population using only seventy

participants (for comparison, the Yeo et al., 2011, Power et al., 2011, and Glasser et al., 2016 papers used between 200 and 1000 participants).

In anticipation of the release of the FunMaps toolbox, we asked just how small we can make our sample size and still get a stable parcellation result. We did this by running FunMaps on random subsamples of different sizes from the seventy TD individuals described above. We found stable cortical and subcortical parcellations across subsamples of thirty, fifty, and seventy participants (Figure 4). These results are very encouraging for our stated goal of offering a parcellation tool that researchers can use on the relatively small sample sizes collected in individual labs. We also ran FunMaps on subsamples of ten and twenty participants and found that these parcellations yielded interpretable results, but identified only coarse networks in the cortex and the parcellation solutions were less stable compared to results from larger sample sizes. However, this does not mean that the toolbox is not usable with sample sizes smaller than thirty participants. Data quality and length of the rs-fMRI run time play critical roles in identifying stable functional networks in the brain (e.g., Gonzalez-Castillo et al., 2014). Thus, collecting more timepoints of rs-fMRI, acquiring data in higher field strengths (e.g., 7 Tesla), and using more sophisticated acquisition sequences (e.g., multi-echo acquisitions – (Cohen et al., 2021) are good ways to increase the likelihood that FunMaps will find optimal functional networks in your brain data (Laumann et al., 2017; Lynch et al., 2020). While we have demonstrated that FunMaps can be used to obtain functional network maps in small groups of individuals, it is worth noting that the toolbox can also be used to find individual-specific network maps, so long as enough data are collected per study participant (e.g., Gordon et al., 2017).

The results described thus far are a product of applying FunMaps to high-quality rs-fMRI data with high tSNR values across the whole brain. To demonstrate the importance of rs-fMRI data quality when identifying stable functional brain networks using rs-fMRI, we ran FunMaps on a group of 450 randomly selected participants from the HCP database. First, we measured the tSNR across the HCP participants and compared it to the seventy participants that were collected in our lab (Figure 5A). The tSNR was significantly lower in the HCP data compared to our data (Figure 5B). Even when using an unpaired t-test to compare the seventy highest tSNR values from the HCP data with our data in cortex and subcortex separately, the difference is pronounced ($cortex_{(138)}$, $t=47.85$, $p<10^{-4}$, $subcortex_{(138)}$, $t=68.84$, $p<10^{-4}$). Not surprisingly, we found that this significant reduction in data quality influenced our ability to find stable functional networks in the HCP data, especially in the subcortex. The agreement curves for the cortical and subcortical masks provide good examples of why it is crucial that users look at the prototypes mapped onto the brain volume (Figure 5C). In the cortical mask, the agreement curves are similar to the agreement curves we get in our lab data (displayed in Figure 1B). However, when we mapped the prototypes to the brain volume, we found that at the 90% threshold (lighter vertical dashed line in Figure 5C), the cortical prototypes are reasonable and similar to the results from our lab example, except that visual regions in the occipital lobe do not separate from the sensorimotor areas in the parietal lobe. At the 93% threshold (darker vertical dashed line in Figure 5C), the prototypes look very similar, but now the visual and sensorimotor areas in the occipital and parietal lobes, respectively, are separate prototypes (Figure 5D). Thus, the 93% threshold is likely the better choice for these data. Meanwhile, we could not find a stable

solution for the subcortical parcellation in this group of 450 HCP participants. As can be seen in the agreement curves, the algorithm did not detect any subcortical network prototypes that met our inclusion criteria until the 85% threshold, then the number of prototypes increased rapidly at subsequent thresholds. This is perhaps not surprising given that the average tSNR in the subcortex mask is 20.5 in the HCP data. However, we do not believe that it is impossible to use FunMaps on subcortical data from HCP or other multi-site fMRI data collection initiatives. These datasets are highly valuable to the field of cognitive neuroscience, and though the data quality is often lower than data that is collected within an individual lab, the sheer number of participants that are provided in these datasets can offset the negative impact of lower tSNR. Here we used a subset of 450 HCP participants, but there are over twelve hundred participants in the HCP database. Increasing the sample size of these data should yield a better outcome than what we present here.

CONCLUSION

We introduced the FunMaps toolbox as a flexible and easy-to-use way of creating topographical maps of functional networks in the human brain using relatively small rs-fMRI datasets that are collected in individual labs. In this paper, we have demonstrated how FunMaps can be used to create stable and replicable multi-level network maps across the whole brain or in focused regions of interest. We developed the FunMaps toolbox to be flexible and easy to use. It is publicly available on GitHub (https://github.com/persichetti-lab/FunMaps) and includes source code for running the

parcellation; auxiliary code for preparing data, evaluating the parcellation, and displaying the results; and further documentation on how to use the toolbox.

METHODS

Demographics. We present data from two separate groups of participants. The main data presented were collected in our lab from seventy typically developing (TD) individuals with no history of psychiatric or neurological disorders [mean (SD) age=19.7 (3.7) years; 19 female]. We also present data demonstrating how to use the FunMaps toolbox on a restricted region of interest (ROI) – i.e., the anterior temporal lobes (ATL). These data were collected in our lab from eighty-eight individuals with no history of psychiatric or neurologic disorders [mean (SD) age, 21.2 years (7.6 years); 24 females]. Seventy of these participants are from the TD group described above. Subsets of the resting-state data from all of the above individuals have been used in several previous studies (Gotts et al., 2012; Jasmin et al., 2019; Persichetti et al., 2021, 2022, 2023; Power et al., 2019; Ramot et al., 2017). Informed assent and consent were obtained from all participants and/or their parent/guardian when appropriate in accordance with a National Institutes of Health (NIH) Institutional Review Board-approved protocol (10-M-0027, clinical trials number NCT01031407). In addition to the data collected in our lab, we also present data from a sample of 450 participants from the Lifespan Human Connectome Project (HCP) Development project [mean (SD) age=16.54 (2.94) years, Range 12-21 years; 231 female] (Somerville et al., 2018).

MRI data acquisition and procedure. For all data collected in our lab, scanning was completed on a General Electric Signa HDxt 3.0 T scanner (GE Healthcare) at the NIH Clinical Center NMR Research Facility. For each participant, T2*-weighted blood oxygen level-dependent (BOLD) images covering the whole brain were acquired using an 8-channel receive-only head coil and a gradient echo single-shot echo planar imaging sequence (repetition time = 3500 ms, echo time = 27 ms, flip angle = 90°, 42 axial contiguous interleaved slices per volume, 3.0-mm slice thickness, 128x128 acquisition matrix, single-voxel volume=1.7x1.7x3.0 mm, field of view = 22 cm). An acceleration factor of 2 (ASSET) was used to reduce gradient coil heating during the session. In addition to the functional images, a high-resolution T1-weighted anatomical image (magnetization-prepared rapid acquisition with gradient echo – MPRAGE) was obtained (124 axial slices, 1.2 mm3 single-voxel volume, 224x224 acquisition matrix, field of view = 24 cm). During the resting scans, participants were instructed to relax and keep their eyes fixated on a central cross. Each resting scan lasted eight minutes and ten seconds for a total of 140 consecutive whole-brain volumes. Independent measures of cardiac and respiratory cycles were recorded during scanning for later artifact removal.

For the HCP Development (HCP-D) data, scanning was completed on 3 T Siemens Prisma scanners (Siemens, Erlangen, Germany). For each participant, T2*-weighted blood oxygen level-dependent (BOLD) images covering the whole brain were acquired using the Siemens 32-channel Prisma head coil and a 2D multiband (MB) gradient-recalled echo (GRE) echo-planar imaging (EPI) sequence (MB8, TR/TE = 800/37 ms, flip angle = 52°) and 2.0 mm isotropic voxels. In addition to the functional images, a high-resolution multi-echoT1-weighted anatomical image (magnetization-

prepared rapid acquisition with gradient echo – MPRAGE) was obtained (Harms et al., 2018; Somerville et al., 2018). The MPRAGE scan used a sagittal FOV of 256×240×166 mm with a matrix size of 320×300×208 slices. Slice oversampling of 7.7% was used, as was 2-fold in-plane acceleration (GRAPPA) in the phase encode direction and a pixel bandwidth of 744 Hz/Px. Other parameters included: TR/TI = 2500/1000, TE = 1.8/3.6/5.4/7.2 ms, flip angle of 8 deg, water excitation employed for fat suppression (to reduce signal from bone marrow and scalp fat), and up to 30 TRs allowed for motion-induced reacquisition. During the resting scans, participants were instructed to stay still, stay awake, and blink normally while looking at the fixation crosshair. Each resting scan lasted six minutes and thirty seconds for a total of 488 consecutive whole-brain volumes. Independent measures of cardiac and respiratory cycles were recorded during scanning for later artifact removal.

Preprocessing. All data that were collected in our lab were preprocessed using the AFNI software package (Cox, 1996). First, the initial three TRs from each EPI scan were removed to allow for T1 equilibration. Next, 3dDespike was used to bound outlying time points in each voxel within 4 SDs of the time series mean, and 3dTshift was used to adjust for slice acquisition time within each volume (to t = 0). 3dvolreg was then used to align each volume of the resting-state scan series to the first retained volume of the scan. White matter and large ventricle masks were created from the aligned MPRAGE scan using Freesurfer (Fischl et al., 2002). These masks were then resampled to EPI resolution, eroded by 1 voxel to prevent partial volume effects with gray matter voxels, and applied to the volume-registered data to generate white matter and ventricle

nuisance regressors before spatial blurring. Scans were then spatially blurred by a 6 mm Gaussian kernel (full-width at half-maximum) and divided by the voxelwise time series mean to yield units of percentage signal change. The data were denoised using the ANATICOR preprocessing approach (Jo et al., 2010). Nuisance regressors for each voxel included the following: six head-position parameter time series (three translation, three rotation), one average eroded ventricle time series, one “localized” eroded white matter time series (averaging the time series of all white matter voxels within a 15-mm radius sphere), eight RETROICOR time series (four cardiac, four respiration) calculated from the cardiac and respiratory measures taken during the scan (Glover et al., 2000), and five respiration volume per time series to minimize end-tidal CO2 effects from deep breaths (Birn et al., 2008). All regressors were detrended with a fourth-order polynomial before denoising, and the same detrending was applied during nuisance regression to the voxel time series. Finally, the residual time series were spatially transformed to standard anatomic space (Talairach–Tournoux) at both 2 and 6 mm3 isotropic resolutions for computational speed in later analyses.

The HCP-D data were preprocessed using the AFNI software package (Cox, 1996). First, 3dDespike was used to bound outlying time points in each voxel within 4 SDs of the time series mean. Next, unWarpEPI was used to warp posterior-anterior (PA) and anterior-posterior (AP) encoding scans to the midpoint of the two scans (each with 478 TRs), simultaneously accomplishing volume registration. The python script align_epi_anat.py was then used to align the MPRAGE scan to the EPI data. White matter and large ventricle masks were created from the aligned MPRAGE scan using Freesurfer (Fischl et al., 2002). These masks were then resampled to EPI resolution,

eroded by 1 voxel to prevent partial volume effects with gray matter voxels, and applied to the volume-registered data to generate white matter and ventricle nuisance regressors before spatial blurring. Scans were then spatially blurred by a 4 mm Gaussian kernel (full-width at half-maximum) and divided by the voxelwise time series mean to yield units of percentage signal change. The data were denoised using the ANATICOR preprocessing approach (Jo et al., 2010). Nuisance regressors for each voxel included the following: six head-position parameter time series (three translation, three rotation), one average eroded ventricle time series, one “localized” eroded white matter time series (averaging the time series of all white matter voxels within a 15-mm radius sphere), and the first 3 PCs of the voxelwise timeseries from the combined white-matter and ventricle masks (modified aCompCor: Behzadi et al., 2007; Stoddard et al., 2016). All regressors were detrended with a fourth-order polynomial before denoising, and the same detrending was applied during nuisance regression to the voxel time series. Following nuisance regression, the PA and AP scans were concatenated, and the residual time series were spatially transformed to standard anatomic space (Talairach–Tournoux) at both 2 and 6 mm3 isotropic resolutions for computational speed in later analyses.

ACKNOWLEDGEMENTS. Research reported in this publication was supported by the National Institute Of Mental Health of the National Institutes of Health under Award Number U01MH109589 and by funds provided by the McDonnell Center for Systems Neuroscience at Washington University in St. Louis. The HCP-Development 2.0 Release data used in this report came from DOI: 10.15154/1520708.

REFERENCES

Behzadi, Y., Restom, K., Liau, J., & Liu, T. T. (2007). A component based noise correction method (CompCor) for BOLD and perfusion based fMRI. *NeuroImage*, *37*(1), 90–101. https://doi.org/10.1016/j.neuroimage.2007.04.042

Birn, R. M., Smith, M. A., Jones, T. B., & Bandettini, P. A. (2008). The respiration response function: The temporal dynamics of fMRI signal fluctuations related to changes in respiration. *NeuroImage*, *40*(2), 644–654. https://doi.org/10.1016/j.neuroimage.2007.11.059

Cohen, A. D., Yang, B., Fernandez, B., Banerjee, S., & Wang, Y. (2021). Improved resting state functional connectivity sensitivity and reproducibility using a multiband multi-echo acquisition. *NeuroImage*, *225*, 117461. https://doi.org/10.1016/j.neuroimage.2020.117461

Cox, R. W. (1996). AFNI: Software for Analysis and Visualization of Functional Magnetic Resonance Neuroimages. *Computers and Biomedical Research*, *29*(3), 162–173. https://doi.org/10.1006/cbmr.1996.0014

Fanselow, M. S., & Dong, H. W. (2010). Are the Dorsal and Ventral Hippocampus Functionally Distinct Structures? In *Neuron* (Vol. 65, Issue 1, pp. 7–19). Cell Press. https://doi.org/10.1016/j.neuron.2009.11.031

Fischl, B., Salat, D. H., Busa, E., Albert, M., Dieterich, M., Haselgrove, C., Kouwe, A. V. D., Killiany, R., Kennedy, D., Klaveness, S., Montillo, A., Makris, N., Rosen, B., & Dale, A. M. (2002). Whole brain segmentation: Automated labeling of neuroanatomical

structures in the human brain. *Neuron*, *33*(3), 341–355. https://doi.org/10.1016/S0896-6273(02)00569-X

Glasser, M. F., Coalson, T. S., Robinson, E. C., Hacker, C. D., Harwell, J., Yacoub, E., Ugurbil, K., Andersson, J., Beckmann, C. F., Jenkinson, M., Smith, S. M., & Essen, D. C. V. (2016). A multi-modal parcellation of human cerebral cortex. *Nature*, *536*(7615), 171–178. https://doi.org/10.1038/nature18933

Glover, G. H., Li, T.-Q., & Ress, D. (2000). Image-based method for retrospective correction of physiological motion effects in fMRI: RETROICOR. *Magnetic Resonance in Medicine*, *44*(1), 162–167. https://doi.org/10.1002/1522-2594(200007)44:1<162::AID-MRM23>3.0.CO;2-E

Gonzalez-Castillo, J., Handwerker, D. A., Robinson, M. E., Hoy, C. W., Buchanan, L. C., Saad, Z. S., & Bandettini, P. A. (2014). The spatial structure of resting state connectivity stability on the scale of minutes. *Frontiers in Neuroscience*, *8*, 138. https://doi.org/10.3389/fnins.2014.00138

Gordon, E. M., Laumann, T. O., Gilmore, A. W., Newbold, D. J., Greene, D. J., Berg, J. J., Ortega, M., Hoyt-Drazen, C., Gratton, C., Sun, H., Hampton, J. M., Coalson, R. S., Nguyen, A. L., McDermott, K. B., Shimony, J. S., Snyder, A. Z., Schlaggar, B. L., Petersen, S. E., Nelson, S. M., & Dosenbach, N. U. F. (2017). Precision Functional Mapping of Individual Human Brains. *Neuron*, *95*(4), 791-807.e7. https://doi.org/10.1016/j.neuron.2017.07.011

Gotts, S. J., Simmons, W. K., Milbury, L. A., Wallace, G. L., Cox, R. W., & Martin, A. (2012). Fractionation of social brain circuits in autism spectrum disorders. *Brain*, *135*(9), 2711–2725. https://doi.org/10.1093/brain/aws160

Grady, C. L. (2020). Meta-analytic and functional connectivity evidence from functional magnetic resonance imaging for an anterior to posterior gradient of function along the hippocampal axis. *Hippocampus*, *30*(5), 456–471. https://doi.org/10.1002/hipo.23164

Harms, M. P., Somerville, L. H., Ances, B. M., Andersson, J., Barch, D. M., Bastiani, M., Bookheimer, S. Y., Brown, T. B., Buckner, R. L., Burgess, G. C., Coalson, T. S., Chappell, M. A., Dapretto, M., Douaud, G., Fischl, B., Glasser, M. F., Greve, D. N., Hodge, C., Jamison, K. W., … Yacoub, E. (2018). Extending the Human Connectome Project across ages: Imaging protocols for the Lifespan Development and Aging projects. *NeuroImage*, *183*, 972–984. https://doi.org/10.1016/j.neuroimage.2018.09.060

Jasmin, K., Gotts, S. J., Xu, Y., Liu, S., Riddell, C. D., Ingeholm, J. E., Kenworthy, L., Wallace, G. L., Braun, A. R., & Martin, A. (2019). Overt social interaction and resting state in young adult males with autism: Core and contextual neural features. *Brain*, *142*(3), 808–822. https://doi.org/10.1093/brain/awz003

Jo, H. J., Saad, Z. S., Simmons, W. K., Milbury, L. A., & Cox, R. W. (2010). Mapping sources of correlation in resting state FMRI, with artifact detection and removal. *NeuroImage*, *52*(2), 571–582. https://doi.org/10.1016/j.neuroimage.2010.04.246

Kalcher, K., Boubela, R. N., Huf, W., Našel, C., & Moser, E. (2015). Identification of Voxels Confounded by Venous Signals Using Resting-State fMRI Functional Connectivity Graph Community Identification. *Frontiers in Neuroscience*, *9*(DEC), 472. https://doi.org/10.3389/fnins.2015.00472

Laumann, T. O., Snyder, A. Z., Mitra, A., Gordon, E. M., Gratton, C., Adeyemo, B., Gilmore, A. W., Nelson, S. M., Berg, J. J., Greene, D. J., McCarthy, J. E., Tagliazucchi, E., Laufs, H., Schlaggar, B. L., Dosenbach, N. U. F., & Petersen, S. E. (2017). On the Stability of BOLD fMRI Correlations. *Cerebral Cortex (New York, N.Y.: 1991)*, *27*(10), 4719–4732. https://doi.org/10.1093/cercor/bhw265

Lynch, C. J., Power, J. D., Scult, M. A., Dubin, M., Gunning, F. M., & Liston, C. (2020). Rapid Precision Functional Mapping of Individuals Using Multi-Echo fMRI. *Cell Reports*, *33*(12), 108540. https://doi.org/10.1016/j.celrep.2020.108540

Marcus, D. S., Harms, M. P., Snyder, A. Z., Jenkinson, M., Wilson, J. A., Glasser, M. F., Barch, D. M., Archie, K. A., Burgess, G. C., Ramaratnam, M., Hodge, M., Horton, W., Herrick, R., Olsen, T., McKay, M., House, M., Hileman, M., Reid, E., Harwell, J., … WU-Minn HCP Consortium. (2013). Human Connectome Project informatics: Quality control, database services, and data visualization. *NeuroImage*, *80*, 202–219. https://doi.org/10.1016/j.neuroimage.2013.05.077

Nadel, L., Hoscheidt, S., & Ryan, L. R. (2013). Spatial cognition and the hippocampus: The anterior-posterior axis. *Journal of Cognitive Neuroscience*, *25*(1), 22–28. https://doi.org/10.1162/jocn_a_00313

Persichetti, A. S., Denning, J. M., Gotts, S. J., & Martin, A. (2021). A Data-Driven Functional Mapping of the Anterior Temporal Lobes. *The Journal of Neuroscience*, *41*(28), 6038–6049. https://doi.org/10.1523/JNEUROSCI.0456-21.2021

Persichetti, A. S., Shao, J., Gotts, S. J., & Martin, A. (2022). Maladaptive Laterality in Cortical Networks Related to Social Communication in Autism Spectrum Disorder. *Journal of Neuroscience*, *42*(48), 9045–9052. https://doi.org/10.1523/JNEUROSCI.1229-22.2022

Persichetti, A. S., Shao, J., Gotts, S. J., & Martin, A. (2023). A functional parcellation of the whole brain in individuals with autism spectrum disorder reveals atypical patterns of network organization. *bioRxiv*, 2023.12.15.571854. https://doi.org/10.1101/2023.12.15.571854

Poppenk, J., Evensmoen, H. R., Moscovitch, M., & Nadel, L. (2013). Long-axis specialization of the human hippocampus. In *Trends in Cognitive Sciences* (Vol. 17, Issue 5, pp. 230–240). Elsevier Current Trends. https://doi.org/10.1016/j.tics.2013.03.005

Power, J. D., Cohen, A. L., Nelson, S. M., Wig, G. S., Barnes, K. A., Church, J. A., Vogel, A. C., Laumann, T. O., Miezin, F. M., Schlaggar, B. L., & Petersen, S. E. (2011). Functional Network Organization of the Human Brain. *Neuron*, *72*(4), 665–678. https://doi.org/10.1016/j.neuron.2011.09.006

Power, J. D., Lynch, C. J., Gilmore, A. W., Gotts, S. J., & Martin, A. (2019). Reply to Spreng et al.: Multiecho fMRI denoising does not remove global motion-associated respiratory signals. In *Proceedings of the National Academy of Sciences of the United States of*

America (Vol. 116, Issue 39, pp. 19243–19244). National Academy of Sciences. https://doi.org/10.1073/pnas.1909852116

Ramot, M., Kimmich, S., Gonzalez-Castillo, J., Roopchansingh, V., Popal, H., White, E., Gotts, S. J., & Martin, A. (2017). Direct modulation of aberrant brain network connectivity through real-time NeuroFeedback. *eLife*, *6*. https://doi.org/10.7554/eLife.28974

Ranganath, C., & Ritchey, M. (2012). Two cortical systems for memory-guided behaviour. In *Nature Reviews Neuroscience* (Vol. 13, Issue 10, pp. 713–726). Nature Publishing Group. https://doi.org/10.1038/nrn3338

Rosvall, M., & Bergstrom, C. T. (2008). Maps of random walks on complex networks reveal community structure. *Proceedings of the National Academy of Sciences*, *105*(4), 1118–1123. https://doi.org/10.1073/pnas.0706851105

Rosvall, M., & Bergstrom, C. T. (2011). Multilevel Compression of Random Walks on Networks Reveals Hierarchical Organization in Large Integrated Systems. *PLoS ONE*, *6*(4), e18209. https://doi.org/10.1371/journal.pone.0018209

Sekeres, M. J., Winocur, G., & Moscovitch, M. (2018). The hippocampus and related neocortical structures in memory transformation. In *Neuroscience Letters* (Vol. 680, pp. 39–53). Elsevier Ireland Ltd. https://doi.org/10.1016/j.neulet.2018.05.006

Somerville, L. H., Bookheimer, S. Y., Buckner, R. L., Burgess, G. C., Curtiss, S. W., Dapretto, M., Elam, J. S., Gaffrey, M. S., Harms, M. P., Hodge, C., Kandala, S., Kastman, E. K., Nichols, T. E., Schlaggar, B. L., Smith, S. M., Thomas, K. M., Yacoub, E., Van Essen, D. C., & Barch, D. M. (2018). The Lifespan Human Connectome Project in

Development: A large-scale study of brain connectivity development in 5-21 year olds. *NeuroImage*, *183*, 456–468. https://doi.org/10.1016/j.neuroimage.2018.08.050

Stoddard, J., Gotts, S. J., Brotman, M. A., Lever, S., Hsu, D., Zarate, C., Ernst, M., Pine, D. S., & Leibenluft, E. (2016). Aberrant intrinsic functional connectivity within and between corticostriatal and temporal-parietal networks in adults and youth with bipolar disorder. *Psychological Medicine*, *46*(7), 1509–1522. https://doi.org/10.1017/S0033291716000143

Talairach, J., Tournoux, P., & Rayport, M. (1997). *Co-planar stereotaxic atlas of the human brain: 3-dimensional proportional system: an approach to cerebral imaging* (Reprint). Thieme [u.a.].

Yeo, B. T. T., Krienen, F. M., Sepulcre, J., Sabuncu, M. R., Lashkari, D., Hollinshead, M., Roffman, J. L., Smoller, J. W., Zöllei, L., Polimeni, J. R., Fisch, B., Liu, H., & Buckner, R. L. (2011). The organization of the human cerebral cortex estimated by intrinsic functional connectivity. *Journal of Neurophysiology*, *106*(3), 1125–1165. https://doi.org/10.1152/jn.00338.2011

FIGURES

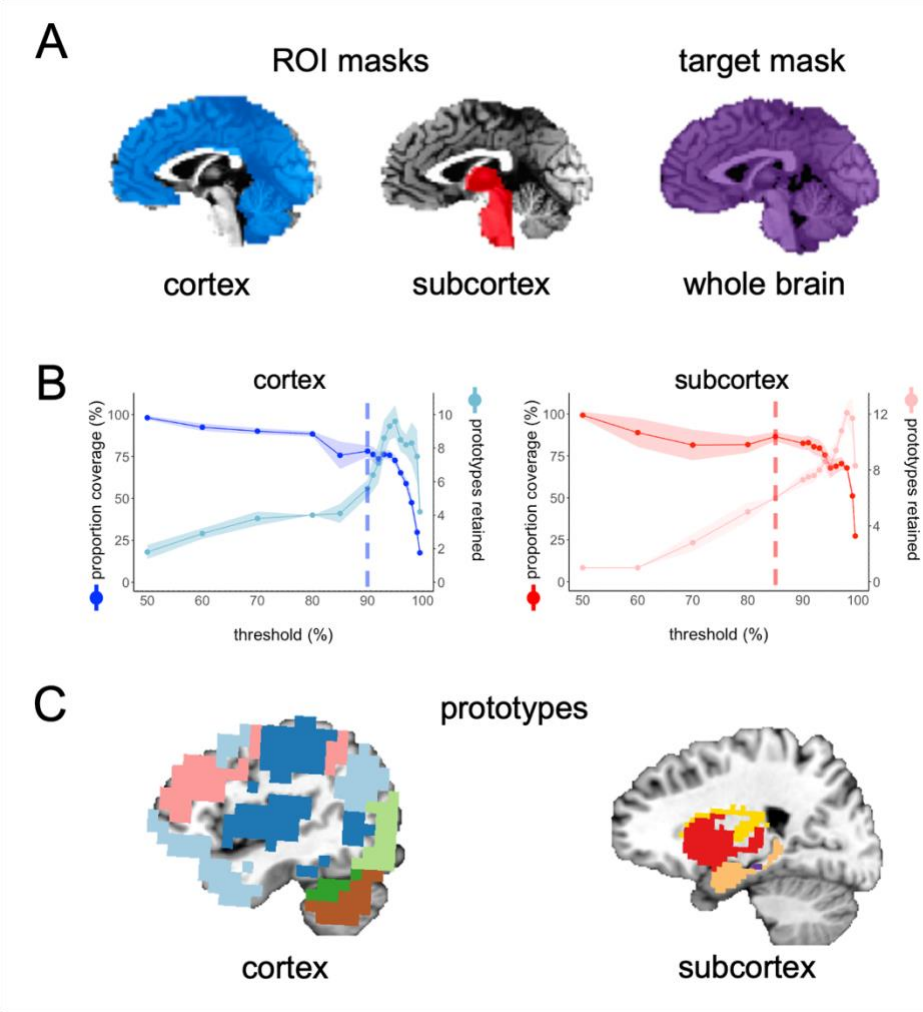

Figure 1. A) In the main example presented in this paper, we chose two ROI masks: a cortical mask that included all cortical and cerebellar voxels (blue) and a subcortical mask that included all voxels in the subcortex (red) and brain stem. Our target mask included all voxels in the whole brain (purple). **B)** The spilt-half agreement curves were constructed across a wide range of thresholds. The error in the line plots represents +/- 1 standard deviation across the ten iterations of the split-half routine. In this example, we chose the 90% threshold in the cortical mask and the 85% threshold for the subcortical mask as the thresholds that maximized proportion of coverage (i.e., number of voxels assigned a network prototype label) and the number of detected network prototypes in each mask (vertical dashed lines). It is critical for the user to evaluate these curves and select thresholds for themselves. **C)** The cortical network prototypes at the 90% threshold and the subcortical prototypes at the 85% threshold. At this stage of the parcellation, the user can map the prototypes back to the volume at select thresholds to evaluate whether they are acceptable before proceeding to the next steps.

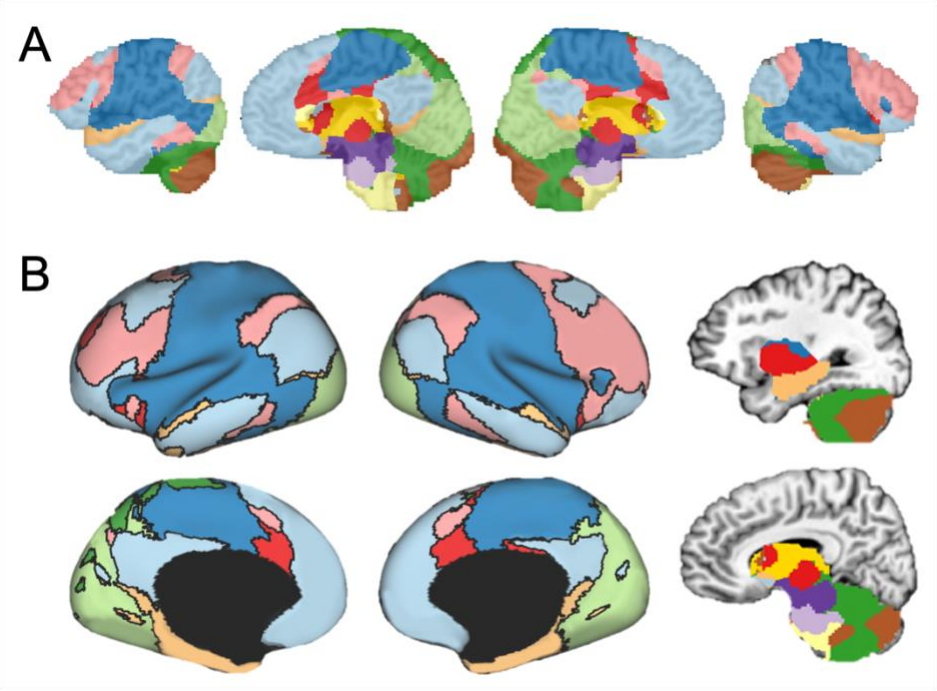

Figure 2. A) The final volumetric network map in the original spatial resolution of the data. **B)** The auxiliary function called *vol2surf.m* can be used to project the network map onto the surface using the HCP Workbench software.

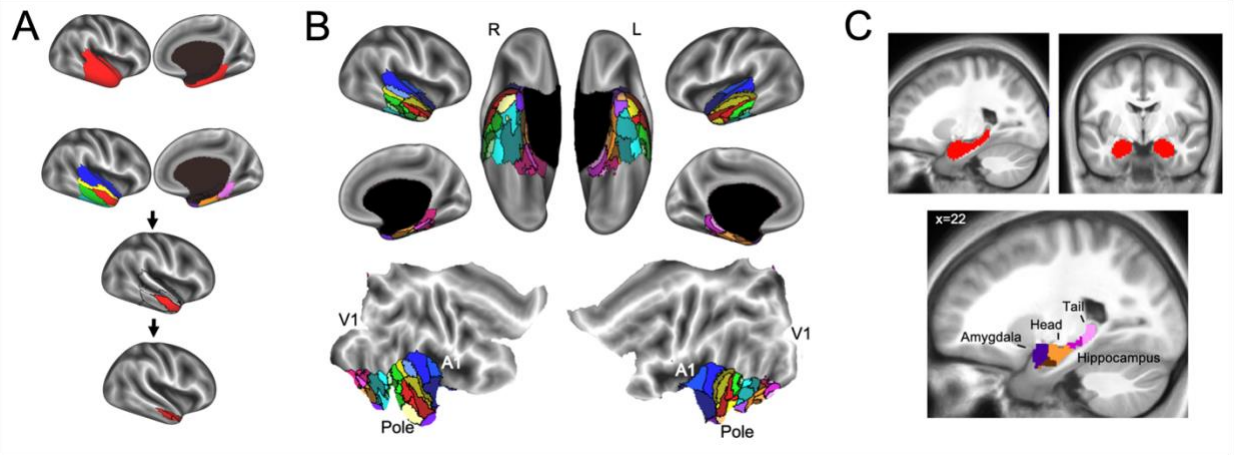

Figure 3. A) The first iteration of the parcellation focused on the cortical (top row) and subcortical masks separately. The cortical mask extended from the anterior tip of the temporal pole back to the Talairach coordinate, y = 35. The subcortical mask included the hippocampus and amygdala. Shown here is an example of how to use FunMaps to create an initial parcellation in the ROI mask and then further parcellate each of the parcels in turn to create a more fine-grained network map. After the first pass of the FunMaps routine, the ATL was divided into eight bilateral parcels (second from top row). We then ran FunMaps again on each of the eight parcels, in turn, to further fractionate each parcel (bottom two rows). **B)** Our parcellation of the ATL resulted in 34 distinct functional parcels based on the patterns of functional connectivity between voxels in the ATL and the rest of the brain. The flat maps in the bottom panel are labeled to orient the reader. V1, primary visual cortex; A1, primary auditory cortex; Pole, temporal pole. **C)** The parcellation within the medial temporal masks (red, top) separated the amygdala (purple) from the hippocampus and further divided the hippocampus into head (orange), body (magenta), and tail (pink). The brown parcel overlaps mostly rhinal cortex and inferolateral hippocampus. This figure is adapted from Persichetti et al., 2021.

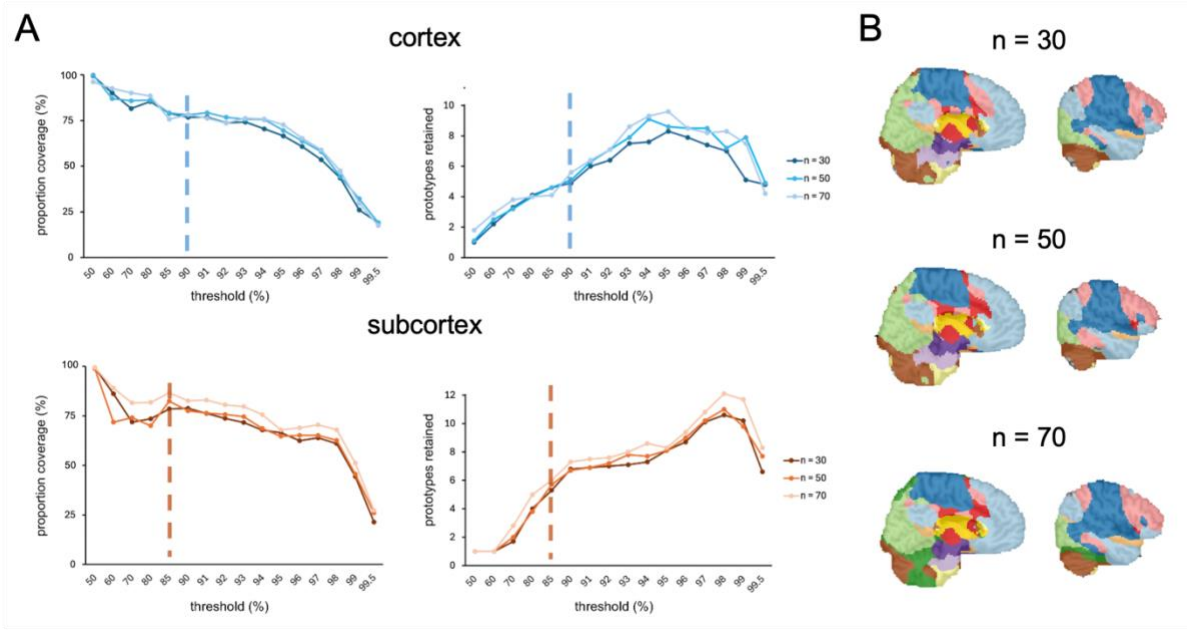

Figure 4. A) The spilt-half agreement curves for sample sizes of 30, 50, and 70 participants. In this example, we chose the 90% threshold in the cortical mask (top) and the 85% threshold for the subcortical mask (bottom) as the thresholds that maximized proportion of coverage (i.e., number of voxels assigned a network prototype label) and the number of detected network prototypes in each mask (vertical dashed lines). **B)** The final volumetric network maps in the original spatial resolution of the data for each sample size.

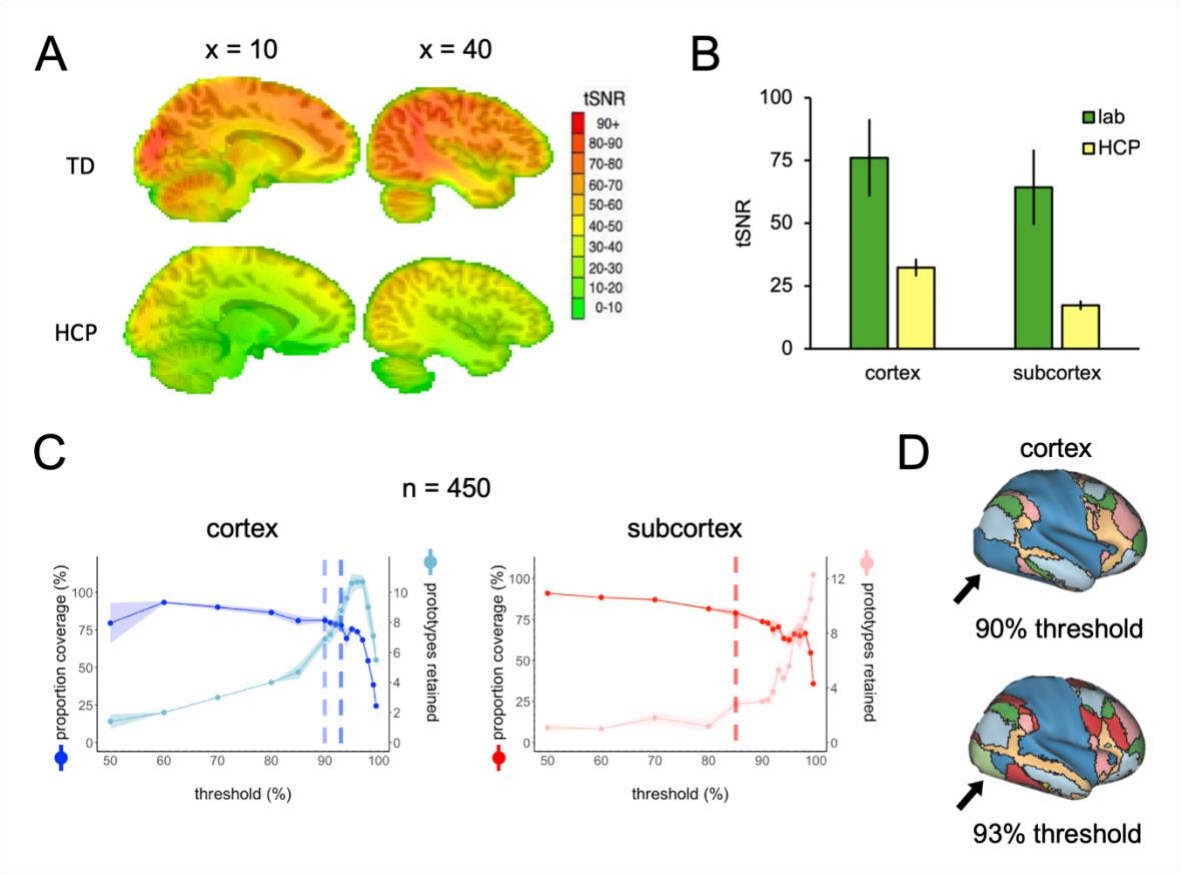

Figure 5. A) Whole-brain tSNR maps averaged across seventy participants from our lab (top) and 450 HCP participants (bottom). **B)** The tSNR values averaged across the cortical and subcortical masks separately in the seventy participants from our lab and the seventy highest tSNR values from the HCP data. **C)** The spilt-half agreement curves across a wide range of thresholds. The error in the line plots represents +/- 1 standard deviation across the ten iterations of the split-half routine. The agreement curves in the cortex are a good example of why it is important to check the protoypes in the brain volume along with looking at the curves. At the 90% threshold (lighter vertical dashed line), the cortical prototypes are reasonable and similar to the results from our lab example, except that visual regions in the occipital lobes do not separate from the sensorimotor areas in the parietal lobe. At the 93% threshold (darker vertical dashed line), the prototypes look very similar, except now the visual and sensorimotor areas in the occipital and parietal lobes, respectively, are now separate prototypes. Meanwhile, the algorithm did not detect any subcortical network prototypes that met our inclusion criteria until the 85% threshold, then the number of prototypes increased rapidly at subsequent thresholds. **D)** When the functional networks are mapped to the cortical surface at the 90% and 93% thresholds, it is clear to see that the visual regions in the occipital lobe do not separate from the sensorimotor areas in the parietal lobe at the 90% threshold, but do separate at the 93% threshold.

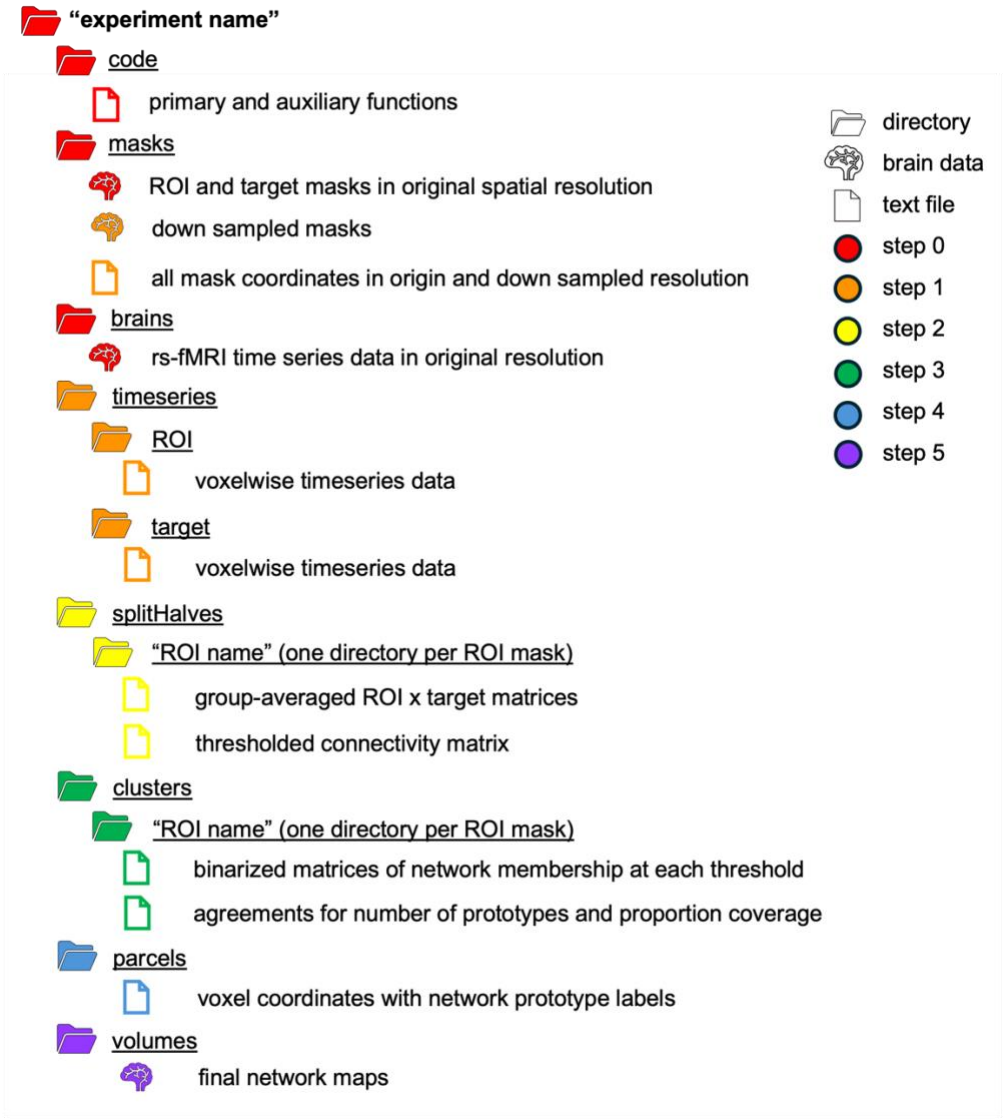

Table 1. A schematic of the directory structure that houses the products of the FunMaps toolbox.